



Article

Compressive Failure Characteristics of a Coal–Rock Combination at Different Angles: Experimental Study and Fractal Analysis

Long Tang ¹, Shihao Tu ^{1,*} , Hongsheng Tu ¹, Kaijun Miao ^{1,*}, Wenlong Li ², Hongbin Zhao ¹, Jieyang Ma ¹ and Lei Zhang ³

¹ State Key Laboratory of Coal Resources and Safe Mining, School of Mines, China University of Mining and Technology, Xuzhou 221116, China; tlwy@cumt.edu.cn (L.T.); 5536@cumt.edu.cn (H.T.); tb21020038b0@cumt.edu.cn (H.Z.); tb20020023b1@cumt.edu.cn (J.M.)

² College of Energy and Mining Engineering, Shandong University of Science and Technology, Qingdao 266590, China; 18361260569@163.com

³ Xuzhou Coal Mining Group, Xuzhou 221018, China; 17768279676@163.com

* Correspondence: tsh@cumt.edu.cn (S.T.); 01140149@cumt.edu.cn (K.M.); Tel.: +86-139-5216-0512 (S.T.)

Abstract: In order to explore the influence of dip angles on the deformation and failure of a coal–rock combination, uniaxial compression experiments were carried out on a coal–rock combination with different dip angles, and the acoustic emissions (hereinafter referred to as AE) responses during loading were collected. Based on the damage mechanics theory and fractal theory, the fractal dimensions of different damage degrees were calculated. The results show that, with the increase in the inclination angle, the compressive strength and elastic modulus of the coal–rock combination gradually decreased, while the AE ringing count gradually increased first and then decreased. At the initial loading stage of the specimen, the greater the damage degree of the coal–rock combination under the same strain condition, the larger the value of its overall fractal dimension. The AE fractal dimension of the coal–rock combination increases gradually between 10% and 20% of the damage degree. It suddenly decreased between 50% and 60%, then increased slightly before gradually decreasing to the minimum between 80% and 100%. The sudden decrease in fractal dimension, a slight increase, and then a continuous decrease can be used as the precursor information for the instability and failure of the coal–rock combination.

Keywords: coal–rock combination; acoustic emission; fractal characteristics; degree of damage



Citation: Tang, L.; Tu, S.; Tu, H.; Miao, K.; Li, W.; Zhao, H.; Ma, J.; Zhang, L. Compressive Failure Characteristics of a Coal–Rock Combination at Different Angles: Experimental Study and Fractal Analysis. *Fractal Fract.* **2024**, *8*, 240. <https://doi.org/10.3390/fractalfract8040240>

Academic Editor: Zine El Abiddine Fellah

Received: 20 March 2024

Revised: 9 April 2024

Accepted: 17 April 2024

Published: 20 April 2024



Copyright: © 2024 by the authors. Licensee MDPI, Basel, Switzerland. This article is an open access article distributed under the terms and conditions of the Creative Commons Attribution (CC BY) license (<https://creativecommons.org/licenses/by/4.0/>).

1. Introduction

The mechanical properties of coal and rock are important parameters in elements of underground engineering, such as coal mine design, roadway support, and coalbed methane mining [1–3]. In coal mining, the roof, coal seam and floor are an organic whole, which leads to the mechanical behavior of an underground coal body being very different from that of laboratory pure coal samples [4,5]. Therefore, many scholars have studied the mechanical properties of coal–rock combinations. Some scholars have studied the strength, burst tendency and failure characteristics of a coal–rock combination through uniaxial and triaxial mechanical experiments [6–8]. Other scholars have analyzed the influencing factors of the mechanical properties of a coal–rock combination, such as the height ratio of the coal–rock [9,10], the dip angle of the coal–rock contact surface [11,12], as well as the loading rate [13,14]. Under the action of external load, the tiny cracks in the rock will close, expand, and penetrate each other after being stressed. In this process, some energy is released in the form of elastic waves, a process known as acoustic emission (hereinafter referred to as AE) [15]. The AE of rock can reflect the damage degree of rock and is directly related to the evolution of internal cracks in rock [16,17]; therefore, some scholars have studied the fracture evolution characteristics of coal–rock combinations by using an AE system [18–20].

The fractal theory was founded by Mandelbrot [21] in the mid-1970s. In 1991, Xie Heping [22] successfully combined damage mechanics with fractal geometry, creating a new field of rock fractal theory research. Subsequently, more and more scholars use fractal theory to study the problems in the mining process. For example, in terms of large scale, Deng et al. [23] used fractal dimension to characterize the distribution and complexity of fractures in mining roadways, recognizing the self-similarity law of fracture distribution in mining rock mass. Wang et al. [24] studied the fractal characteristics of an overburden fracture network under the condition of upward mining, obtaining the relationship between the width of the working face and the fractal dimension of the fracture network. Miao et al. [25] studied the fractal evolution characteristics of overlying rock fractures under gully water bodies, obtaining the variation law of fractal dimension of overlying rock fractures under different mining height conditions.

For small scale, Li et al. [26] studied the energy evolution and fractal characteristics of a fractured coal–rock combination under impact load. Kong et al. [27] carried out a triaxial compression test on coal containing methane, collecting the AE response in the loading process. On this basis, the fractal dimension of the AE time series was calculated, and it was concluded that the AE response and fractal dimension can reflect the evolution of cracks in the loading process. Wu et al. [28] and Gao et al. [29] studied the AE and fractal characteristics of different lithology and water-bearing coal samples during the fracture process, obtaining the relationship between the fractal dimension and the mechanical properties of the samples.

In summary, domestic and foreign scholars have achieved fruitful results in the study of the mechanical properties of coal–rock assemblages, while the application of fractal theory to the mechanical properties of coal–rock assemblages is relatively less, and there are few studies on the fractal characteristics of AE of ‘rock–coal–rock’ combination damage with different dip angles. However, the occurrence conditions of coal seams in Chinese coal mines are complicated, and the inclination of coal seams in some coal mines varies greatly, while the mechanical properties of coal–rock combinations are different under different inclination conditions. Therefore, this paper will combine the fractal theory to study the AE characteristics of different damage degrees of coal–rock combinations with different dip angles in the process of uniaxial compression, discussing the precursor information of coal–rock instability and failure in order to provide a theoretical basis for engineering applications such as roadway support in abnormal dip areas of coal mines.

2. AE Experiment of Coal–Rock Combination

2.1. Background and Specimen Preparation

The dip angle of the coal seam in the 74104 working face of the Zhangshuanglou Coal Mine in Xuzhou City, Jiangsu Province, China, varies greatly, about 10° – 35° , with an average dip angle of 23° . The roof and floor of the working face are fine sandstone. The stress of the roadway surrounding rock with different coal seam dip angles is different, and its deformation and failure characteristics are also different. In order to explore the deformation and failure characteristics of a coal–rock combination with different dip angles in the process of compression, and to facilitate the design of roadway support while using the Zhangshuanglou Coal Mine as the background, the roof, coal seam, and floor rock samples of the 74104 working face were processed and made into ‘rock–coal–rock’ combination specimens by high-strength dolomite glue according to the order of rock strata for a uniaxial compression test, as shown in Figure 1.

According to the international rock mechanics test specification, the diameter of the composite specimen is 50 mm, the height is 100 mm, and the non-parallelism of the two ends of the specimen is less than 0.05 mm [30]. The mechanical test specimens of the coal–rock combination with coal seam inclinations of 0° , 15° , 25° , 35° , and 45° were designed, and the coal thickness is 20 mm. In order to compare with the mechanical characteristics of single coal and rock specimens, the preparation of and experimentation on single coal and rock specimens were also carried out, and the number of each test specimen was three.

Specimens should be numbered before the experiment, and the numbering sequence of single coal bodies and rock mass is M-1, M-2, M-3, Y-1, Y-2, Y-3, respectively. The numbering order of coal–rock combination with different dip angles is MY-0°-1, MY-0°-2, MY-0°-3, and so on to MY-45°-1, MY-45°-2, MY-45°-3. The numbering is shown in Figure 1, and the test scheme is shown in Table 1.

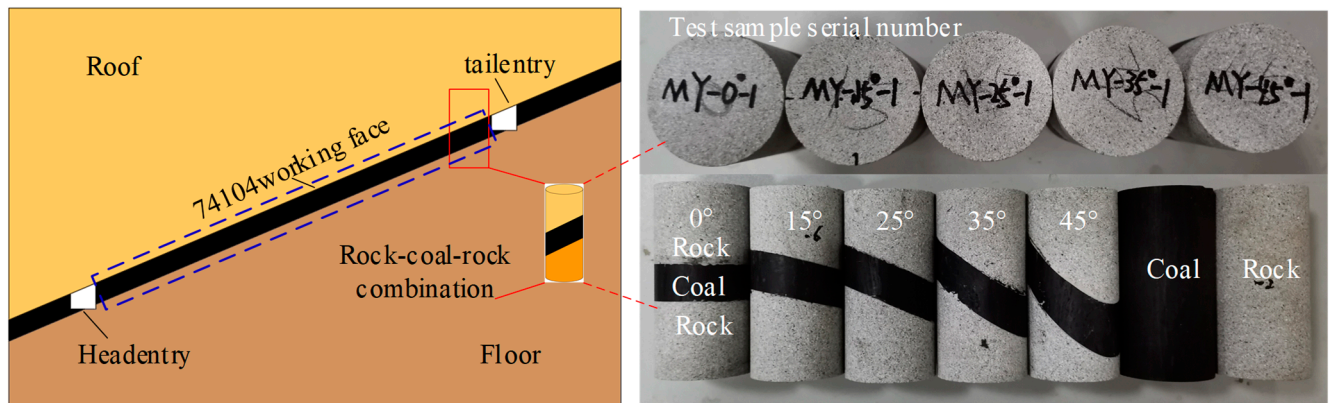


Figure 1. Coal–rock combination and number schematic diagram.

Table 1. Experimental scheme of coal–rock combination with different dip angles.

| Group Number of Test Piece | Lithology | Dip Angle/(°) | Specimen Number |
|----------------------------|--------------------------------------|---------------|-------------------|
| 1 | Coal | 0 | M-1~M-3 |
| 2 | Fine sandstone | 0 | Y-1~Y-3 |
| 3 | Fine sandstone -coal- fine sandstone | 0 | MY-0°-1~MY-0°-3 |
| 4 | Fine sandstone -coal- fine sandstone | 15 | MY-15°-1~MY-15°-3 |
| 5 | Fine sandstone -coal- fine sandstone | 25 | MY-25°-1~MY-25°-3 |
| 6 | Fine sandstone -coal- fine sandstone | 35 | MY-35°-1~MY-35°-3 |
| 7 | Fine sandstone -coal- fine sandstone | 45 | MY-45°-1~MY-45°-3 |

2.2. Experimental Equipment and Equipment Parameter Settings

As shown in Figure 2, the whole experiment system mainly includes the Express-8 AE acquisition system (ANALYSIS, San Francisco, CA, USA) and load control system, among which the Express-8 AE acquisition system mainly includes an AE probe, pre-amplifier, a high-speed data acquisition instrument, a computer and other equipment, while the loading control system mainly includes a WAW-600 press (CHEN XIN, Jinan, China), a servo controller, a computer and other equipment. The loading control system adopts displacement loading mode, and the loading rate is 0.2 mm/min. In the AE acquisition system, the threshold value is set to 50 dB, the peak identification time is set to PDT = 50 μ s, the impact identification time is set to HDT = 200 μ s, and the impact lock time is set to HLT = 300 μ s.

AE probes are arranged in the middle of the coal–rock combination and in the upper and lower rock mass, with a total of 6 AE probes. In order to ensure full contact between AE probes and specimens and good signal reception, Vaseline (ANALYSIS, San Francisco, CA, USA) is applied between AE probes and specimens to make full contact between them, as shown in the physical diagram in Figure 2.

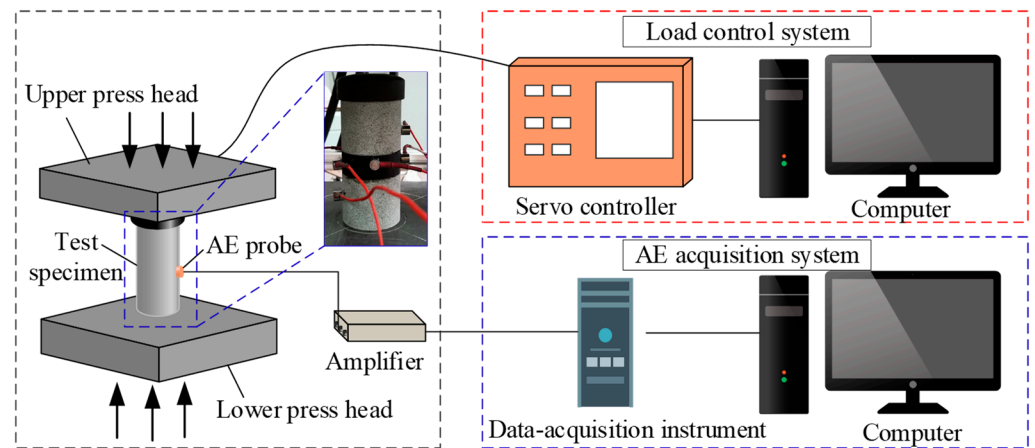


Figure 2. Experimental system diagram.

3. Experimental Result Analysis of Coal–Rock Combination

3.1. Deformation and Failure Characteristics

After the uniaxial compression test, the typical failure modes of a single coal body, rock mass, and a coal–rock combination with different dip angles are shown in Figure 3.

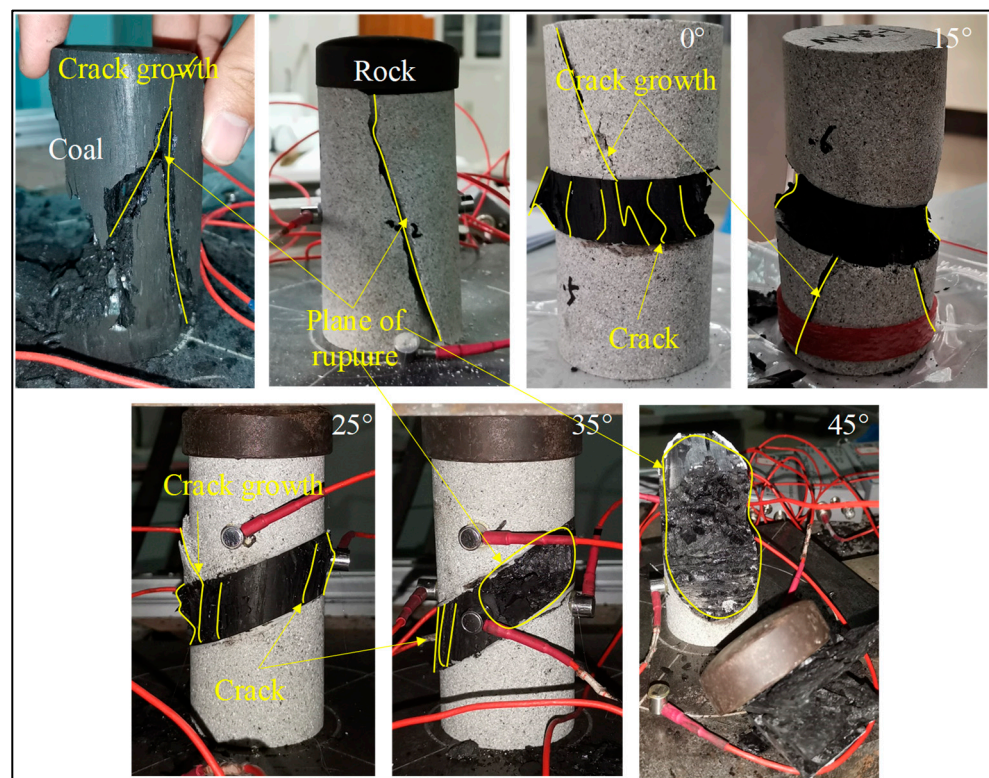


Figure 3. Typical deformation and failure patterns of specimens under uniaxial compression.

As can be seen from Figure 3, a single coal body is subjected to shear and tensile failure under uniaxial compression, resulting in a shear failure plane and columnar splitting plane. In addition, the coal body is loose, porous, has low strength and is relatively broken after failure. Shear failure occurs mainly in single rock masses due to their high strength.

Because the tensile strength of the rock is far less than the compressive strength, the coal body in the 0° coal–rock combination is subjected to tension failure, mainly in the form of columnar splitting failure. After the coal body is damaged, cracks spread to the top and bottom rock mass, resulting in weak plane shear failure of the top and bottom rock mass.

Affected by the dip angle, the upper and lower ends of the 15° coal–rock combination first produce cracks, damage, and spalling, and the damage degree is larger than that of the middle part, resulting in a cone-like damage pattern. The upper and lower ends of the coal body in the 25° coal–rock combination are first damaged by tension, with the upper and lower ends of the coal body extruding outward while the cracks at the lower end extend to the roof rock mass. In the 35° coal–rock combination, there may be primary cracks in the middle and upper parts of the coal body, which are the first subjected to compression, shear failure, spalling, while tensile failure occurs in the lower part, resulting in a large number of cracks. Due to the large inclination angle of the 45° coal–rock combination, the coal–rock mass mainly slips near the coal–rock interface.

It can be seen that, in the coal–rock combination body, due to the low strength of the coal body, the coal body first produces cracks, damage, and weak surface spalling. The cracks then gradually expand to the roof and floor rock mass, resulting in weak surface shear failure; with the increase in the coal seam dip angle, the coal–rock combination gradually changes from tensile-shear failure to slip failure.

3.2. Mechanical Characteristics

After organizing the experimental stress and strain data, the stress–strain curves of a single coal body, rock mass, and a coal–rock combination of different angles during the failure process can be obtained, as shown in Figure 4.

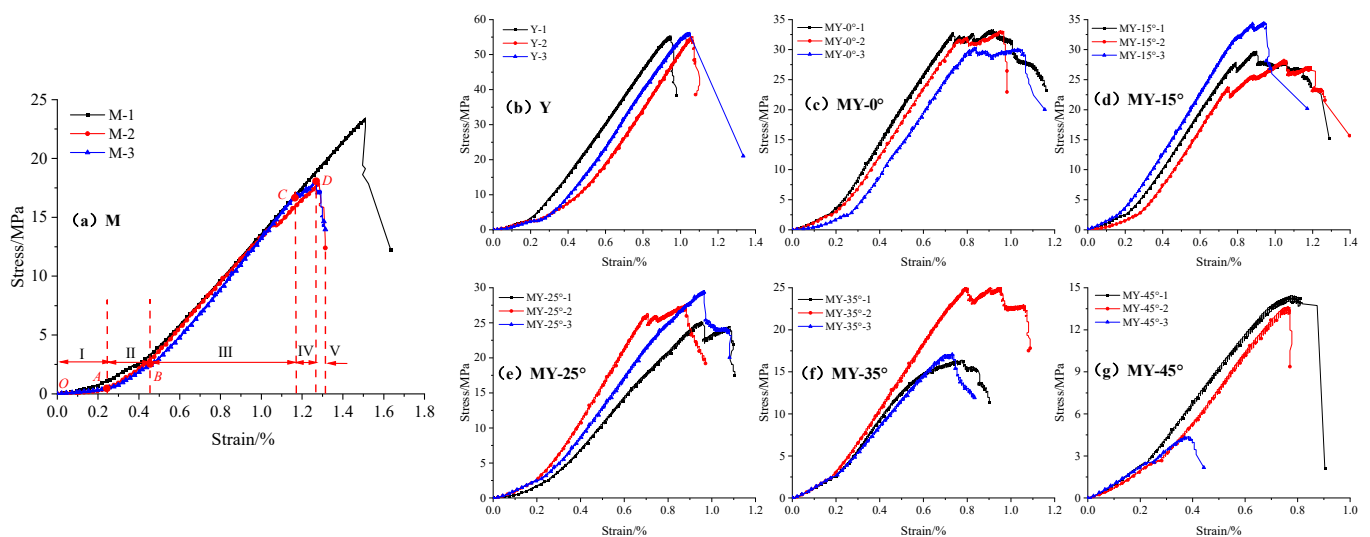


Figure 4. Stress–strain curve of specimens.

Taking the stress–strain curve of M-3 specimen in Figure 4a as an example, the stress and deformation analysis of coal and rock mass is carried out. It can be seen from the figure that the deformation and failure of the coal and rock mass are divided into the following five stages: pore compaction stage I (OA section), elastic deformation stage II (AB section), micro-fracture stable development stage III (BC section), unstable fracture development stage IV (CD section), and post-fracture stage V (after point D). Comparing the stress–strain curves of a single coal body, rock mass and coal–rock combination at different dip angles, it can be seen that the stress–strain curves of the single rock mass and 45° coal–rock combination have no obvious unstable fracture development stage IV. The unstable fracture development stage IV of single coal body is shorter, and the unstable fracture development stage IV of the 0°–35° coal–rock combination is relatively longer. It is shown that the failure of a single hard rock mass and 45° coal–rock combination is sudden and transient, followed by coal, and the 0°–35° coal–rock combination.

According to the stress and strain data in Figure 4 and Formula (1), the average maximum axial stress, strain and elastic modulus of a single coal body, rock mass and

coal–rock combination with different dip angles can be obtained, as shown in Table 2. According to Table 2, the change curve shown in Figure 5 can be drawn.

$$E = \frac{\sigma}{\varepsilon} \quad (1)$$

where: E is the rock elastic modulus, MPa; σ is the axial stress at any point on the axial stress–strain curve, and MPa; ε is the axial strain corresponding to σ .

Table 2. The average maximum axial stress, strain and elastic modulus of different types of coal–rock combinations.

| Specimen Types | Average Maximum Axial Stress/MPa | Average Maximum Axial Strain/% | Average Elastic Modulus/GPa |
|----------------|----------------------------------|--------------------------------|-----------------------------|
| M | 19.75 | 1.42 | 1.93 |
| Y | 55.44 | 0.85 | 6.97 |
| MY-0° | 32.23 | 1.10 | 5.17 |
| MY-15° | 30.76 | 1.28 | 4.50 |
| MY-25° | 27.40 | 1.05 | 3.93 |
| MY-35° | 19.40 | 0.94 | 3.33 |
| MY-45° | 10.73 | 0.70 | 1.99 |

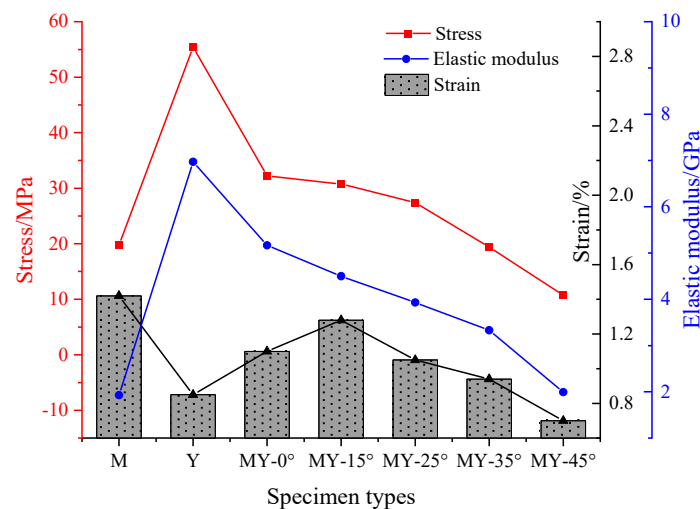


Figure 5. The average stress, strain and elastic modulus of different types of specimens.

It can be seen from M (coal body), Y (rock mass), and MY-0° (0° coal–rock combination) in Figure 5 that the strength and elastic modulus of rock mass > coal–rock combination > coal body, and the strain of rock mass < coal–rock combination < coal body. According to the data change trend line of the coal–rock combination with different dip angles (MY-0°~MY-45°) in the diagram, the average ultimate compressive strength and elastic modulus of the coal–rock combination gradually decrease with the increase in coal seam dip angle, and the average maximum strain increases first and then decreases gradually. At 15°, the average maximum strain is the largest, and the average maximum strain decreases gradually after 15°.

3.3. AE Characteristics

A large number of studies have shown that the AE ringing count is one of the characteristic parameters that can better reflect the change of material properties, which is proportional to the strain energy released by crack propagation and fracture in materi-

als [31]. Therefore, this paper takes the real-time and cumulative ringing count of AE as the characteristic parameters, utilizing the 0° coal–rock combination as an example (Figure 6) to analyze the AE characteristics of the specimen under uniaxial compression. The AE real-time and cumulative ringing count evolution characteristics of other specimens are shown in Figure 7.

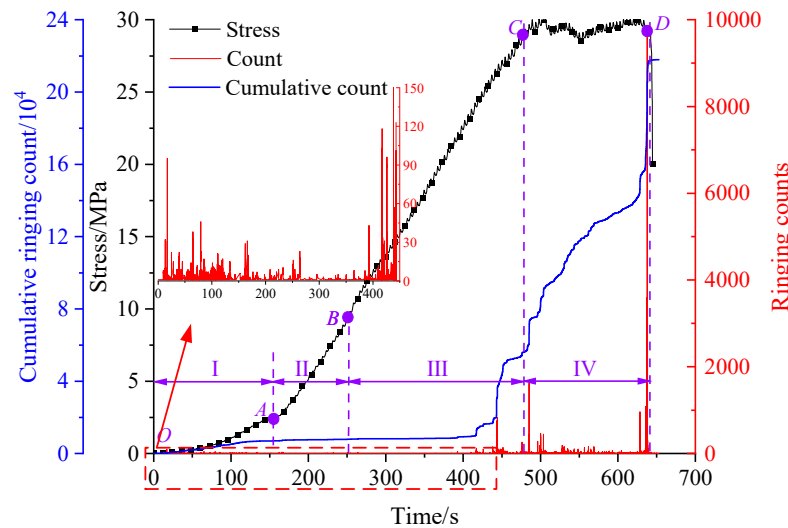


Figure 6. The relationship between specimen load, real-time and cumulative ringing counts and time (0° coal–rock combination).

From Figure 6, it can be seen that, on the basis of the analysis of the deformation and the failure stage of the above-mentioned specimen, from the perspective of the AE ringing count, during the loading process of the specimen, the AE ringing count in the pore compaction stage (I) is less, while the AE ringing count in the unstable fracture development stage (IV) is the most. On the whole, the ringing count increases with the increase in stress. When the specimen breaks, the ringing count shows a stage continuous or jump-type increase. The larger number of ringing is the embodiment of crack propagation and energy release. During the loading process, the cumulative ringing count of the specimen gradually increased, and the area with the largest increase was the late stage of microfracture stable development (III) and the stage of unstable fracture development. The cumulative count of the final ringing in the stable development stage of micro-rupture is 0.56×10^4 , and the cumulative count of the final ringing in the unstable rupture development stage is about 21.77×10^4 , which is 7.05% and 3.88% higher than the cumulative count of the final ringing in the previous stage. From the time point of view, the time period of the pore compaction stage is 0–154 s and the time is 154 s, while the time period of the elastic deformation stage (II) is 154–252 s and the time is 98 s. The time period of the stable development stage of the micro-fracture is 252–479 s and the time is 227 s. Additionally, the time period of the unstable rupture development stage is 479–641 s, which takes 162 s.

In conclusion, in the pore compaction stage, due to the closure of internal micro-cracks, fewer new cracks are generated, and the real-time and cumulative ringing counts of AE are minimal. In the elastic deformation stage, the elastic energy began to be stored inside the specimen in the early stage, and the original cracks began to expand while micro-cracks began to sprout in the later stage. The AE ringing count was small, and this stage took the shortest time. In the stable development stage of the micro-fracture, micro-cracks gradually expand, and the real-time and cumulative ringing counts of AE gradually increase. In the late stage of this stage, micro-cracks occur, and the real-time and cumulative ringing counts of AE increase abruptly, which takes the longest time. In the development stage of unstable fractures, a large number of macroscopic cracks occur, and the final penetration leads to the failure of the specimen. In this stage, the real-time and cumulative AE ringing counts are the most.

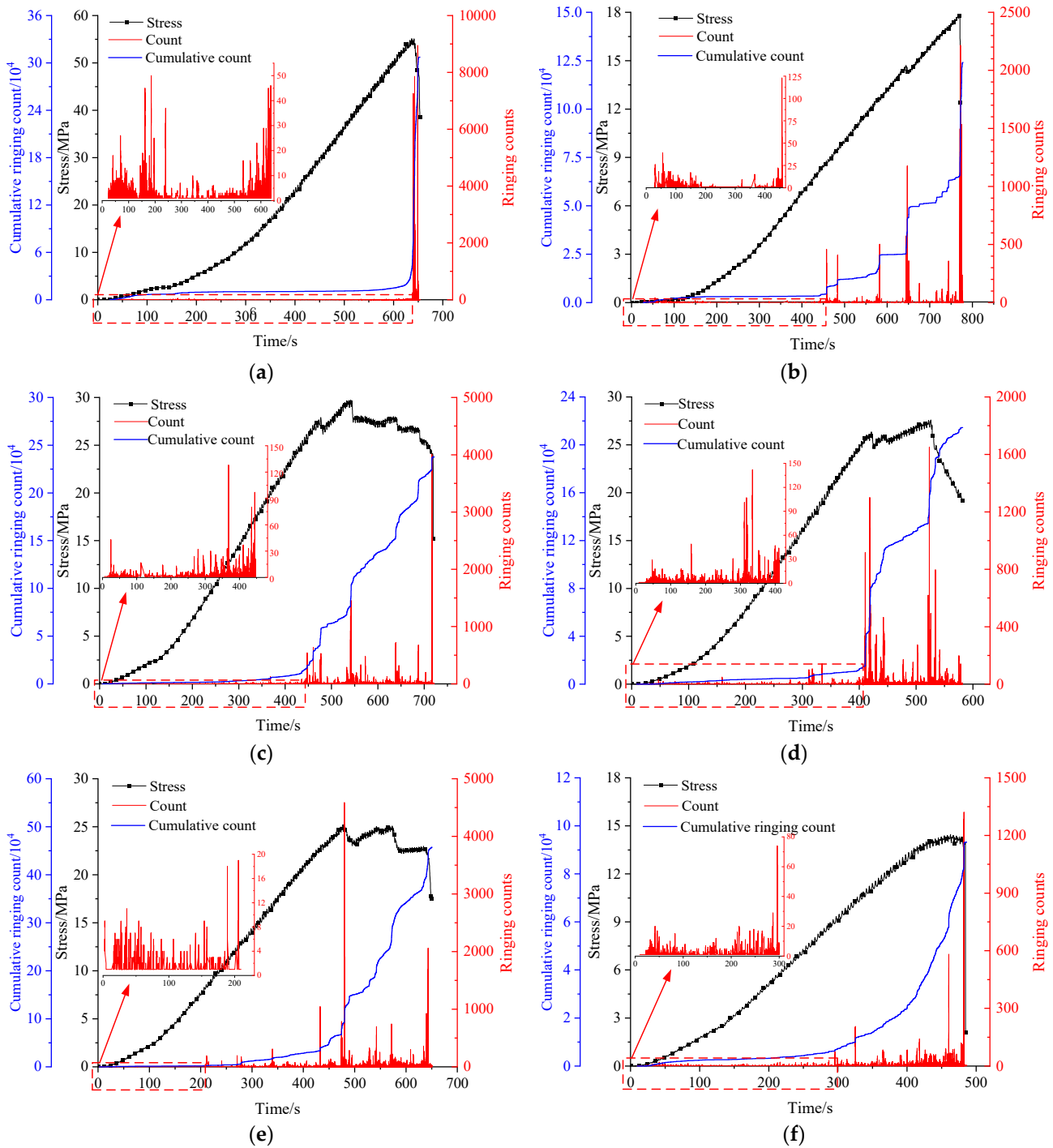


Figure 7. The relationship between specimen load, real-time and cumulative ringing counts and time (0° coal–rock combination). (a) Single rock mass. (b) Single coal body. (c) 15° coal–rock combination. (d) 25° coal–rock combination. (e) 35° coal–rock combination. (f) 45° coal–rock combination.

From Figure 7a,b, it can be seen that the unstable fracture development stage of a single coal (rock) specimen takes a short time, especially a single rock specimen, which is basically a moment, indicating that the sandstone has high strength and accumulates a large amount of elastic energy. This is an instantaneous release, so its AE ringing count is very low in the first few stages, and its AE ringing count increases sharply during the near-failure period. The ringing count reaches the maximum value at the moment of failure, and the cumulative ringing count is about 30.62×10^4 . The coal body is relatively loose and porous, and the AE ringing count is intermittently increased in the stable development stage of micro-fracture

and the unstable fracture development stage. Compared with the rock mass, the number of cracks is more, and the cumulative ringing count is about 12.41×10^4 . According to the analysis of Figure 6, the cumulative ringing count of a single rock mass specimen $> 0^\circ$ coal–rock combination $>$ single coal body, indicating that the elastic energy released by the rock mass failure of the specimen $> 0^\circ$ coal–rock combination $>$ single coal body.

Combined with Figures 6 and 7c,d, it can be seen that, with the increase in the dip angle of the coal–rock combination, the cumulative count of AE ringing of the specimen increases gradually at first and then decreases. When the dip angle of the coal–rock combination is 35° , the cumulative count of AE ringing is the largest, and the cumulative count of ringing is about 45.77×10^4 . The unstable fracture development stage of the specimen gradually decreases with the increase in the inclination angle of the coal–rock combination. Combined with the deformation and failure characteristics of the specimen (Figure 3), it can be seen that the main reason is the coal–rock interface being affected by the inclination angle, which makes the force change. When the inclination angle of the coal–rock combination exceeds 35° , the failure mode gradually changes from tensile shear failure to slip failure.

4. AE Fractal Characteristics of Coal–Rock Combination Damage

4.1. AE Characteristics of Coal–Rock Combination Damage

Damage mechanics originated from the concepts of continuity factor and effective stress proposed by Kachanov [32]. Rabotnov [33] proposed damage variable D when studying metal creep, as shown in the following equation.

$$D = \frac{A_d}{A} \quad (2)$$

where A_d is the cross-sectional area of the rock sample that is compressed, the generation, expansion, convergence, penetration, and until the macroscopic damage of the new crack, while A is the cross-sectional area of the initial non-damage. $D = 0$ is the state of non-destructive material; $D = 1$ is the complete failure state of the material; $0 < D < 1$ is the state of different damage degree of the material.

Let the cumulative ringing count of AE when the whole section A of the non-destructive material is completely destroyed be C_0 , then the ringing count of AE when the unit area is destroyed is C_w :

$$C_w = \frac{C_0}{A} \quad (3)$$

When the cross-section damage area reaches A_d , the cumulative AE ringing count C_d is:

$$C_d = C_w A_d = \frac{C_0}{A} A_d \quad (4)$$

The combined Formulas (1) and (3) can be obtained:

$$D = \frac{C_d}{C_0} \quad (5)$$

From Formula (5), the relationship between stress, damage variable D and the strain of the single coal body, rock mass, and coal–rock combination with different dip angles can be obtained, as shown in Figure 8.

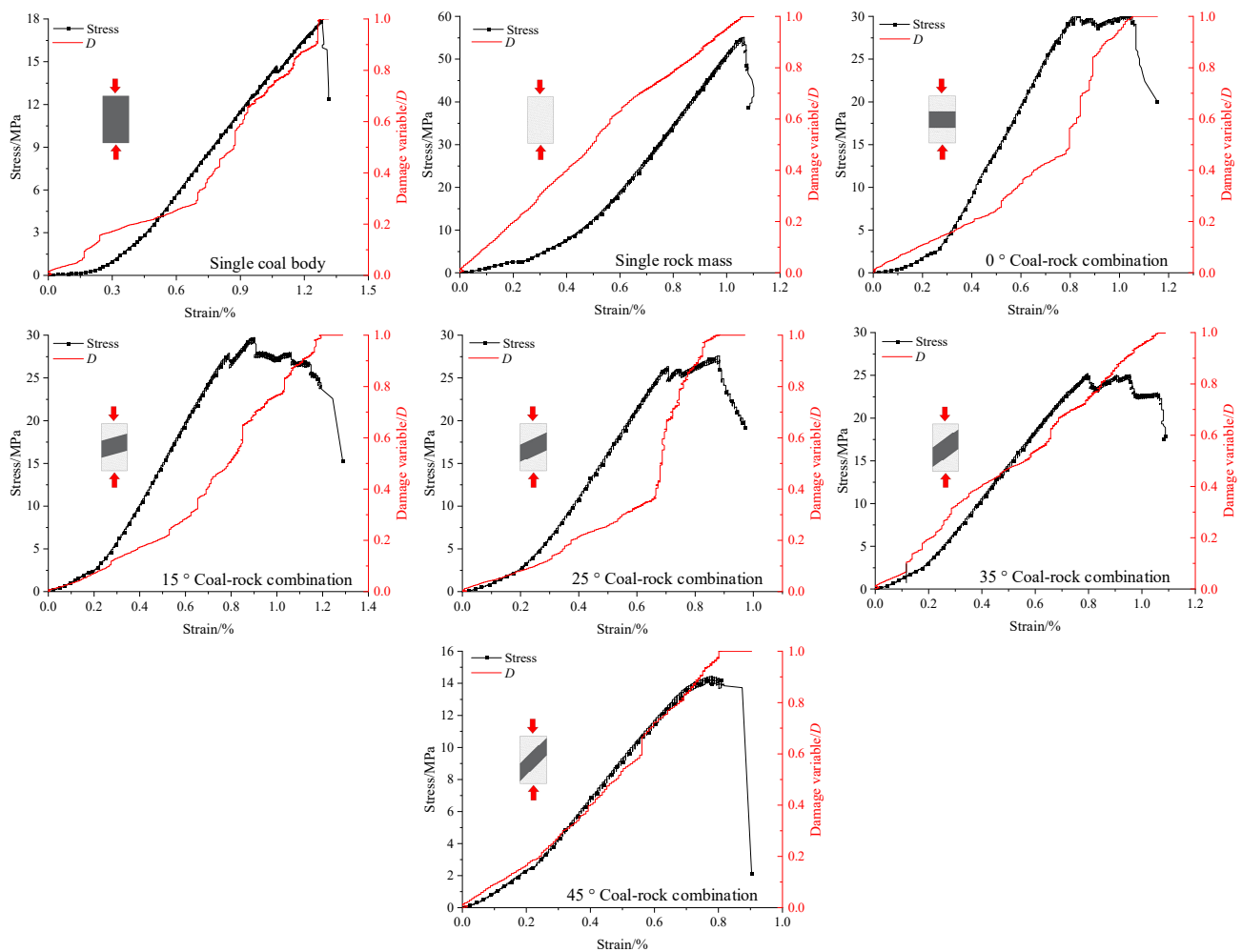


Figure 8. The relationship between stress, damage variable and strain of different types of specimens.

It can be seen from Figure 8 that the damage variable D of the specimen gradually increases with the increase in the strain of the specimen, and the increase in different stress growth stages is different. Based on the deformation and failure stages divided by the stress–strain curve of the specimen in Figure 4a, the average damage variable increases in different types of specimens in different deformation and failure stages are counted, as shown in Table 3.

Table 3. The increase in damage variable (D) in different deformation and failure stages of different types of specimens.

| Specimen Types | Average Damage Variable (D) Increase/% | | | |
|---------------------------|--|---------------------------|--|------------------------------------|
| | Pore Compaction Stage | Elastic Deformation Stage | Microfracture Stable Development Stage | Unstable Rupture Development Stage |
| Single coal body | 57 | 27 | 96 | 120 |
| Single rock mass | 96 | 105 | 111 | 106 |
| 0° coal–rock combination | 52 | 42 | 100 | 175 |
| 15° coal–rock combination | 35 | 50 | 83 | 150 |
| 25° coal–rock combination | 39 | 56 | 139 | 189 |
| 35° coal–rock combination | 88 | 123 | 82 | 104 |
| 45° coal–rock combination | 86 | 121 | 136 | 173 |

It can be seen from Table 3 that the increase in the damage variable of the specimen is basically the smallest in the pore compaction stage and the largest in the unstable fracture development stage. The increase in the damage variable of the single rock mass as a whole $>0^\circ$ coal–rock combination $>$ single coal mass. With the increase in the dip angle of the coal–rock combination, the increase in the damage variable in the pore compaction stage and the elastic deformation stage of the specimen gradually increases. This shows that, under the same strain condition at the initial stage of loading, the greater the inclination angle, the greater the damage degree of the coal–rock combination.

4.2. AE Fractal Characteristics of Coal–Rock Combination

The fractal theory was created in the 1970s. After continuous improvement and application by scholars, it has been widely used in physics, geology, material science, and engineering technology. In physics, fractal dimension is widely used to study various natural phenomena and physical problems. For example, in fluid mechanics, fractal dimension can be used to describe complex fluid dynamics structures, such as turbulence. In physical chemistry, fractal dimension can be used to describe the complex surface structure and the properties of porous media. In materials science, fractal dimension can be used to study the structure and properties of materials [28]. The calculation methods of fractal dimension mainly include the Hausdorff dimension, information dimension, Minkovsky dimension, and correlation dimension. Among them, the correlation dimension is relatively widely used. The commonly used calculation method for the correlation dimension of the time series is the G-P algorithm [29,34], so this paper has chosen this method to calculate the fractal dimension value.

Taking the AE ringing count sequence as the research object, each AE ringing count sequence corresponds to a sequence set X_n with a capacity of n , as shown in the following formula:

$$X_n = \{x_1, x_2, \dots, x_n\} \quad (6)$$

where, x_i is the basic parameter of acoustic emission, $i = 1 \sim n$. The Formula (6) can form an m -dimensional vector space. First, take the number of m as a vector in the m -dimensional space, denoted by:

$$A_1 = \{x_1, x_2, \dots, x_m\} \quad (7)$$

Then, move a data backwards, take m to form the second space vector, and so on; a total of $N = n - m + 1$ vectors are formed. The corresponding correlation function is shown as follows:

$$C_m(r) = \frac{1}{N^2} \sum_{i=1}^N \sum_{j=1}^N H(r - \|A_i - A_j\|) \quad (8)$$

where H is the Heaviside function, expressed as follows:

$$H(x) = \begin{cases} 1(x > 0) \\ 0(x \leq 0) \end{cases} \quad (9)$$

A_i and A_j are the i and j vectors; r is the given scale, and to avoid dispersion, r takes the following values:

$$r = k \frac{1}{N^2} \sum_{i=1}^N \sum_{j=1}^N \|A_i - A_j\| \quad (10)$$

where: k is the scale coefficient. When $k \leq 0.1$, the AE fractal characteristics are not obvious, so the values in this paper are 0.2, 0.4, 0.6, 0.8, 1.0, 1.2, 1.4 [30].

For a given r , there is always a corresponding correlation function $C_m(r)$ corresponding to it, and the corresponding values are depicted in the log-log coordinate system to obtain $(\lg C_m(r), \lg r)$, respectively taking different k , and obtaining multiple sets of coordinate values in the log-log coordinate system. The obtained coordinate values are performed by

unary linear regression, and the slope of the regression function is the fractal dimension. Its calculation formula is as follows:

$$F = \lim_{r \rightarrow 0} \frac{\ln C_m(r)}{\ln r} \tag{11}$$

Using the 2023 version of MATLAB to process the AE ringing count sequence obtained by different types of specimens during uniaxial compression, phase space reconstruction and correlation dimension calculation, the fractal dimension of different types of specimens under different damage degrees is obtained, as shown in Table 4.

Table 4. Fractal dimension of different damage degree of different types of specimens.

| Specimen Types | Fractal Dimension of Different Damage Degree | | | | | | | | | |
|---------------------------|--|-------|-------|-------|-------|-------|-------|-------|-------|-------|
| | 10% | 20% | 30% | 40% | 50% | 60% | 70% | 80% | 90% | 100% |
| Single coal body | 0.682 | 0.827 | 0.520 | 0.106 | 0.092 | 0.558 | 0.043 | 0.115 | 0.248 | 0.217 |
| Single rock mass | 0.726 | 0.484 | 0.360 | 0.194 | 0.912 | 1.152 | 0.85 | 0.957 | 0.300 | 0.228 |
| 0° coal–rock combination | 0.244 | 0.560 | 0.500 | 0.320 | 0.040 | 0.029 | 0.057 | 0.192 | 0.175 | 0.014 |
| 15° coal–rock combination | 0.387 | 0.466 | 0.190 | 0.438 | 0.068 | 0.038 | 0.034 | 0.063 | 0.046 | 0.006 |
| 25° coal–rock combination | 0.562 | 0.293 | 0.223 | 0.384 | 0.639 | 0.083 | 0.102 | 0.073 | 0.067 | 0.040 |
| 35° coal–rock combination | 1.241 | 1.296 | 1.140 | 0.202 | 0.074 | 0.250 | 0.011 | 0.008 | 0.066 | 0.045 |
| 45° coal–rock combination | 0.563 | 0.943 | 1.437 | 0.674 | 0.495 | 0.083 | 0.454 | 0.233 | 0.168 | 0.021 |

In order to analyze the variation law of fractal dimension between various specimens under the different damage degrees. According to Table 4, the fractal dimension change curves between coal body, rock mass, and coal–rock combination body, and the fractal dimension change curves between the coal–rock combination bodies with different dip angles are drawn, respectively, as shown in Figure 9.

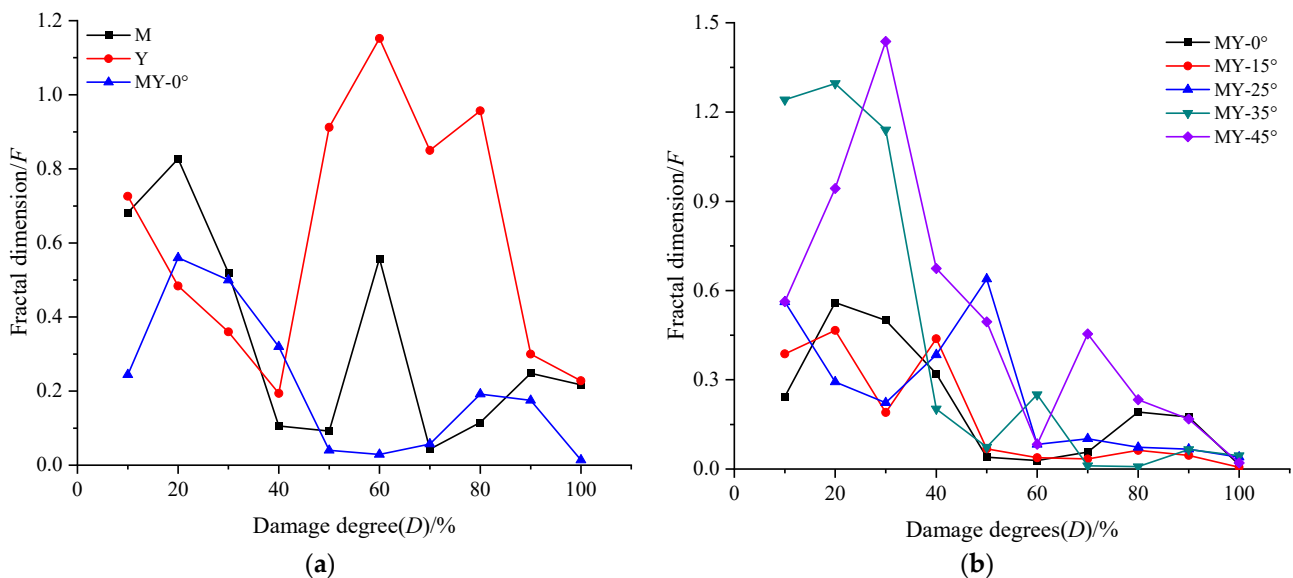


Figure 9. Variation trend of fractal dimension of various specimens under different damage degrees. (a) Coal, rock mass and 0° coal–rock combination. (b) Coal–rock combination with different dip angles.

From Figure 9, it can be seen that the AE ringing count fractal dimension values of the specimens under different damage degrees are different. On the whole, the AE ringing

count fractal dimension of the specimens gradually increases between 10% and 20% of the damage degree. There was a sudden drop between 50% and 60%, and there was a certain increase after that, with it gradually decreasing to the lowest value between 80% and 100%. It can be seen from Figure 9a that the fractal dimension of AE ringing count of rock mass in the process of deformation and failure is obviously different from that of coal and the 0° coal–rock combination. Because the rock mass is dense siltstone, its primary pores are few and the hardness is large. In the process of deformation and failure, the AE ringing count is less, so its overall fractal dimension is larger than that of coal and the 0° coal–rock combination. From Figure 9b, it can be seen that, with the increase in the inclination angle of the coal–rock combination, the fractal dimension value of the whole coal–rock combination is larger, especially when the inclination angle of the coal–rock combination is 35° and above, and the increase is the largest. This is due to the gradual transformation of its deformation and failure form from tensile shear failure to slip failure, and the AE ringing count is greatly reduced, which is consistent with the above experimental analysis.

In order to more clearly understand the relationship between the fractal dimension of the AE ringing count and the AE ringing count and stress during the deformation and failure process of the specimen, the fractal dimension of the acoustic emission ringing count, the AE count, and the relationship between stress and time during the deformation and failure process of the specimen are drawn, as shown in Figure 10.

It can be seen from Figure 10 that the AE ringing count of the specimen increases with the gradual increase in the loading stress. The fractal dimension of the AE ringing count is larger when the AE ringing count is less. When the stress increases to a certain value, the specimen highlights a large number of cracks, and the AE ringing count increases suddenly, while the fractal dimension of the AE ringing count decreases suddenly. During the period when the specimen is about to be destroyed, the AE ringing count increases frequently in a jumping way and the fractal dimension of the AE is gradually lower, indicating that there is a good correspondence between the fractal dimension of the AE ringing count, the AE count, and the stress during the deformation and failure of the specimen. Therefore, the fractal dimension of the AE sequence decreases suddenly, then increases slightly, then decreases continuously as the precursor information of the instability and failure of the coal–rock combination.

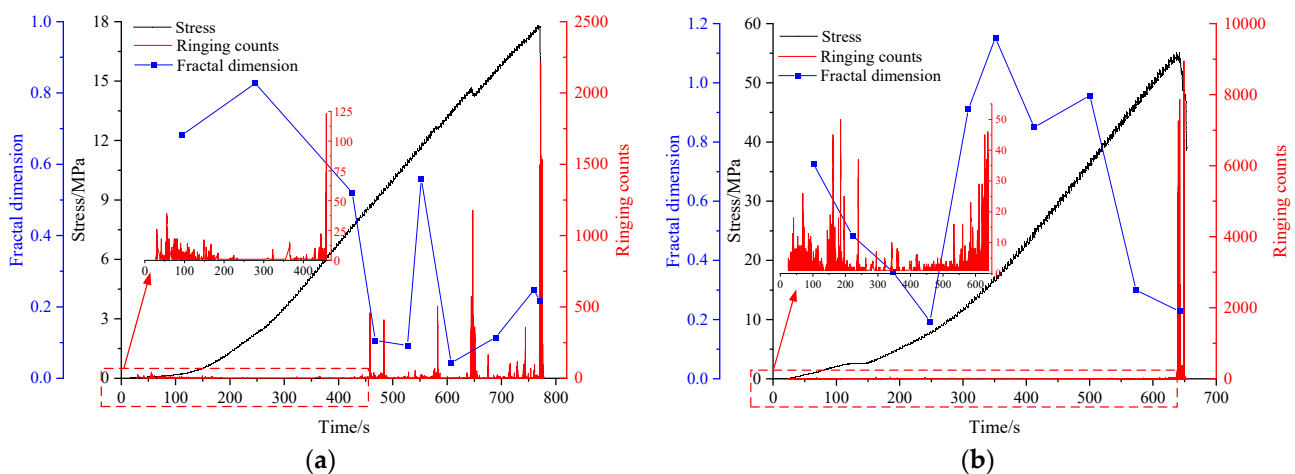


Figure 10. Cont.

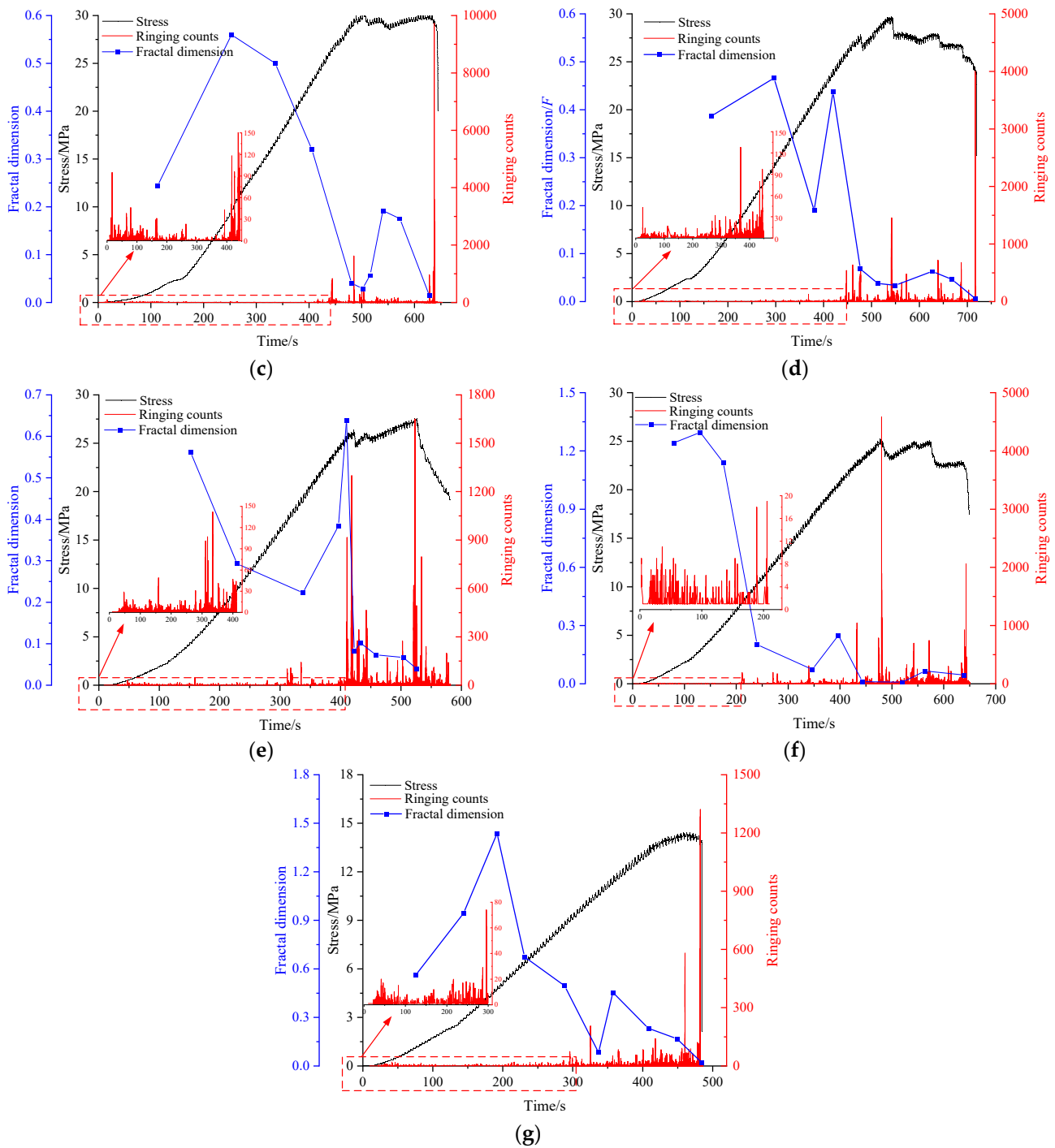


Figure 10. Fractal dimension, AE ringing count, stress and time relation curve. (a) Single rock mass. (b) Single coal body. (c) 0° coal–rock combination. (d) 15° coal–rock combination. (e) 25° coal–rock combination. (f) 35° coal–rock combination. (g) 45° coal–rock combination.

5. Discussion

The research results show that the fractal dimension of the acoustic emission sequence of the damage of the coal–rock combination during the uniaxial compression process corresponds to its deformation and failure characteristics, while the change law of the fractal dimension can be used as an information precursor for the deformation and failure of the coal–rock combination. With the increase in dip angle, the mechanical properties of the coal–rock combination gradually decrease, the acoustic emission ringing count gradually decreases, the fractal dimension gradually increases, and the deformation and

failure characteristics change, gradually transferring from tensile-shear failure to slip failure.

Combined with the experimental results and the deformation and failure characteristics of the roadway surrounding rock in the 74104 working face (Figure 11), it can be seen that:

- (1) The compressive strength and elastic modulus of the fine sandstone of the roof and floor are greater than those of the coal body, which leads to the failure of the coal body on both sides of the roadway under the action of mining stress, and the cracks gradually expand to the roof and floor strata. In addition, the strain of the coal body is greater than that of the rock mass. In the deformation of the surrounding rock of the roadway, the coal body deforms greatly and squeezes into the roadway, as shown in Figure 11a.
- (2) In the coal and rock mass on both sides of the roadway, affected by the dip angle of the coal seam, the strength, strain, and elastic modulus of the coal–rock combination gradually decrease with the increase in the dip angle of the coal seam, indicating that the greater the dip angle of the coal seam, the more easily the coal and rock mass on both sides of the roadway is damaged.
- (3) Combined with the failure characteristics of the coal–rock combination, it can be seen that, under the influence of dip angle, the combination first produces cracks, damage, and spalling from the upper and lower ends of the coal body, while the main damage position is located on the contact surface of the coal–rock. Corresponding to the high side of the roadway, the sharp corner is prone to damage, as shown in Figure 11c.



Figure 11. Deformation and failure characteristics of surrounding rock of right-angle trapezoidal roadway on site.

In summary, it can be seen that the support of the right-angle trapezoidal roadway in the abnormal dip angle area is mainly at the junction of the coal and rock of the roadway and the corner of the roadway. With the increase in the dip angle of the coal seam, the bearing energy of the high-level surrounding rock on both sides of the roadway is lower, which is prone to slip failure. The research results provide a theoretical basis for roadway support under this condition, but some problems are worthy of further discussion:

- (1) In the process of underground mining in coal mines, most of the underground surrounding rock is in a three-dimensional stress state, especially in deep mining, which is more obvious and cannot be ignored [15]. Therefore, the fractal characteristics of AE of coal–rock combination damage in the process of triaxial compression should be further studied.
- (2) In addition to the dip angle of the coal–rock interface, the height ratio of coal to rock, lithology, and the loading rate of the loading system in the coal–rock combination will also affect the deformation and failure of the coal–rock combination, and its AE fractal characteristics will also be different [8,13,14]. Therefore, the fractal characteristics of the AE of the influencing factors of deformation and failure of the coal–rock combination can be further studied.
- (3) In addition to the fractal characteristics of the AE sequence, the deformation and failure of the coal–rock combination can also be analyzed by the fractal dimension of the broken particle size before and after the coal–rock combination test [26]. A variety of fractal dimension calculation methods can be used for further comparative analysis.
- (4) Through experiments, it is concluded that the fractal characteristics of acoustic emission can well-reflect the damage evolution and failure of a coal–rock combination. Similarly, fractal analysis can be carried out in combination with mine microseismic monitoring data, so as to monitor and warn the deformation and failure of underground surrounding rock [35,36].

6. Conclusions

The main conclusions are as follows:

- (1) The strength and elastic modulus of rock mass > coal–rock combination > coal body, and the strain of rock mass < coal–rock combination < coal body; the compressive strength and elastic modulus of coal–rock combination gradually decrease with the increase in dip angle.
- (2) The cumulative count of the AE ringing of the coal–rock combination increases first and then decreases with the increase in dip angle. The cumulative count of ringing is the largest at 35°, as, after that, the failure form of the combination gradually changes from tensile shear failure to slip failure.
- (3) The increase in damage variable of the specimen is basically the smallest in the pore compaction stage and the largest in the unstable fracture development stage. The increase in the damage variable of a single rock mass as a whole > 0° coal–rock combination > single coal mass. With the increase in the inclination angle of the coal–rock combination, the increase in the damage variable in the pore compaction stage and the elastic deformation stage of the specimen increases gradually.
- (4) The fractal dimension of the AE ringing count of the coal–rock combination gradually increases when the damage degree is 10–20%. There is a sudden drop between 50% and 60%, and then there is a small increase, which gradually decreases to the lowest value between 80% and 100%. The fractal dimension of the AE sequence can be slightly increased and then continuously reduced as the precursor information of the instability and failure of the coal–rock combination. With the increase in the inclination angle, the fractal dimension of the whole coal–rock combination is larger.

Author Contributions: Conceptualization, L.T. and S.T.; methodology, W.L. and L.Z.; software, H.Z. and L.T.; validation, J.M., L.T., K.M., and H.T.; formal analysis, L.T. and K.M.; writing—original draft preparation, L.T.; writing—review and editing, S.T. and H.T.; project administration, S.T. All authors have read and agreed to the published version of the manuscript.

Funding: This research was funded by the National Natural Science Foundation of China (No. 51874281), the National Natural Science Foundation for Young Scientists of China (No. 52004270).

Data Availability Statement: The data presented in this study are available on request from the corresponding author.

Acknowledgments: We are very grateful for the support of the research team and the generous help of the engineering and technical staff of the Zhangshuanglou Coal Mine.

Conflicts of Interest: Author Lei Zhang was employed by the company Xuzhou Coal Mining Group. The remaining authors declare that the research was conducted in the absence of any commercial or financial relationships that could be construed as a potential conflict of interest.

Glossary

| | |
|--------------------------|--|
| A_d | the cross-sectional area of the specimen with damage, m^2 |
| A | the cross-sectional area of the specimen at initial no damage, m^2 |
| D | damage variable |
| C_0 | the cumulative acoustic emission ringing count when the entire section A of the undamaged material is completely destroyed |
| C_w | acoustic emission ringing count at unit area microelement failure |
| C_d | Cumulative acoustic emission ringing count |
| x_i | the basic parameter of acoustic emission, $i = 1 \sim n$ |
| H | the Heaviside function |
| X_i | the i vectors |
| X_j | the j vectors |
| r | the given scale |
| k | the scale coefficient |
| C_m | correlation function |
| AE | acoustic emission |
| E, σ, ε | elastic modulus, stress, strain |

References

- Chen, Y.; Zuo, J.; Liu, D.; Wang, Z. Deformation failure characteristics of coal–rock combined body under uniaxial compression: Experimental and numerical investigations. *Bull. Eng. Geol. Environ.* **2019**, *78*, 3449–3464. [[CrossRef](#)]
- Ma, S.; Liu, K.; Guo, T.; Yang, J.; Li, X.; Yan, Z. Experimental and numerical investigation on the mechanical characteristics and failure mechanism of cracked coal & rock-like combined sample under uniaxial compression. *Theor. Appl. Fract. Mech.* **2022**, *122*, 103583.
- Liu, X.; Tan, Y.; Ning, J.; Lu, Y.; Gu, Q. Mechanical properties and damage constitutive model of coal in coal–rock combined body. *Int. J. Rock Mech. Min. Sci.* **2018**, *110*, 140–150.
- Lei, S.; Hao, D.; Cao, S. Study on uniaxial compression deformation and fracture development characteristics of weak interlayer coal–rock combination. *Fractal Fract.* **2023**, *7*, 731. [[CrossRef](#)]
- Song, H.; Zuo, J.; Liu, H.; Zuo, S. The strength characteristics and progressive failure mechanism of soft rock–coal combination samples with consideration given to interface effects. *Int. J. Rock Mech. Min. Sci.* **2021**, *138*, 104593. [[CrossRef](#)]
- Liu, J.; Wang, E.; Song, D.; Wang, S.; Niu, Y. Effect of rock strength on failure mode and mechanical behavior of composite samples. *Arab. J. Geosci.* **2015**, *8*, 4527–4539. [[CrossRef](#)]
- Zuo, J.; Song, H. Energy evolution law and differential energy instability model of coal–rock combined body. *J. China Coal Soc.* **2022**, *47*, 3037–3051.
- Zuo, J.; Chen, Y.; Cui, F. Investigation on mechanical properties and rock burst tendency of different coal–rock combined bodies. *J. China Univ. Min. Technol.* **2018**, *47*, 81–87.
- Yang, E.; Li, S.; Lin, H.; Zhao, P.; Qin, L.; Zhao, B. Influence mechanism of coal thickness effect on strength and failure mode of coal–rock combination under uniaxial compression. *Environ. Earth Sci.* **2022**, *81*, 429. [[CrossRef](#)]
- Ma, B.; Wang, F.; Liu, H.; Yin, D.; Xia, Z. Mechanical properties of rock–coal–rock composites at different inclined coal seam thicknesses. *Front. Phys.* **2022**, *9*, 806055.
- Guo, D.; Zuo, J.; Zhang, Y.; Yang, R. Research on strength and failure mechanism of deep coal–rock combination bodies of different inclined angles. *Rock Soil Mech.* **2011**, *32*, 1333–1339.
- Wu, Y.; Yan, Z.; Luo, S.; Tang, Y.; Wang, T.; Cao, J. Dip effect of stress transfer and structural instability mechanism of coal–rock combination. *Coal Sci. Technol.* **2023**, *51*, 105–116.
- Wang, K.; Du, F.; Zhang, X.; Wang, L.; Xin, C. Mechanical properties and permeability evolution in gas-bearing coal–rock combination body under triaxial conditions. *Environ. Earth Sci.* **2017**, *76*, 815. [[CrossRef](#)]
- Huang, B.; Liu, J. The effect of loading rate on the behavior of samples composed of coal and rock. *Int. J. Rock Mech. Min. Sci.* **2013**, *61*, 23–30. [[CrossRef](#)]
- Yang, Y.; Wang, D.; Guo, M.; Li, B. Study of rock damage characteristics based on acoustic emission tests under triaxial compression. *Chin. J. Rock Mech. Eng.* **2014**, *33*, 98–104.

16. Shkuratnik, V.; Filimonov, Y.; Kuchurin, S. Regularities of acoustic emission in coal samples under triaxial compression. *J. Min. Sci.* **2005**, *41*, 44–52. [[CrossRef](#)]
17. Wang, X.; Liu, X.; Wang, E.; Li, X.; Zhang, X.; Zhang, C.; Kong, B. Experimental research of the AE responses and fracture evolution characteristics for sand-paraffin similar material. *Constr. Build. Mater.* **2017**, *132*, 446–456. [[CrossRef](#)]
18. Aker, E.; Kühn, D.; Vavryčuk, V.; Soldal, M.; Oye, V. Experimental investigation of acoustic emissions and their moment tensors in rock during failure. *Int. J. Rock Mech. Min. Sci.* **2014**, *70*, 286–295. [[CrossRef](#)]
19. Moradian, Z.; Ballivy, G.; Rivard, P.; Gravel, C.; Rousseau, B. Evaluating damage during shear tests of rock joints using acoustic emissions. *Int. J. Rock Mech. Min. Sci.* **2010**, *47*, 590–598. [[CrossRef](#)]
20. Li, F.; Yin, D.; Wang, F.; Jiang, N.; Li, X. Effects of combination mode on mechanical properties of bi-material samples consisting of rock and coal. *J. Mater. Res. Technol.* **2022**, *19*, 2156–2170. [[CrossRef](#)]
21. Mandelbrot, B. *Fractals: Forms, Chance and Dimension*; W. H. Freeman: San Francisco, CA, USA, 1977.
22. Xie, H. *Introduction to Fractal-Rock Mechanics*; Science Press: Beijing, China, 1996; pp. 136–137.
23. Deng, G.; Xie, H.; Gao, M.; Li, C.; He, Z. Numerical simulation on the evolution of mining-induced fracture network in a coal seam and its overburden under the top coal caving method. *Adv. Civ. Eng.* **2020**, *2020*, 8833193. [[CrossRef](#)]
24. Wang, C.; Zhang, N.; Han, Y.; Xiong, Z.; Qian, D. Experiment research on overburden mining-induced fracture evolution and its fractal characteristics in ascending mining. *Arab. J. Geosci.* **2015**, *8*, 13–21. [[CrossRef](#)]
25. Miao, K.; Tu, S.; Tu, H.; Liu, X.; Li, W.; Zhao, H.; Tang, L.; Ma, J.; Li, Y. Research on fractal evolution characteristics and safe mining technology of overburden fissures under gully water body. *Fractal Fract.* **2022**, *6*, 486. [[CrossRef](#)]
26. Li, C.; Xu, Y.; Zhang, Y.; Li, H. Study on energy evolution and fractal characteristics of cracked coal-rock-like combined body under impact loading. *Chin. J. Rock Mech. Eng.* **2019**, *38*, 2231–2241.
27. Kong, X.; Wang, E.; Hu, S.; Shen, R.; Li, X.; Zhan, T. Fractal characteristics and acoustic emission of coal containing methane in triaxial compression failure. *J. Appl. Geophys.* **2016**, *124*, 139–147. [[CrossRef](#)]
28. Wu, X.; Liu, X.; Liang, Z.; You, X.; Yu, M. Experimental study of fractal dimension of AE serialsof different rocks under uniaxial compression. *Rock Soil Mech.* **2012**, *33*, 3561–3569.
29. Gao, B.; Li, H.; Li, L.; Su, C. Acoustic emission and fractal characteristics of saturated coal samples in the failure process. *J. Min. Saf. Eng.* **2015**, *32*, 665–676.
30. Guo, H.; Song, D.; He, X.; Lou, Q.; Qiu, L. Fractal characteristics of acoustic emission in different damage degrees of impact coal. *Coal Sci. Technol.* **2021**, *49*, 38–46.
31. Li, D.; Wang, E.; Kong, X.; Wang, X.; Zhang, C.; Jia, H.; Wang, H.; Qian, J. Fractal characteristics of acoustic emissions from coal under multi-stage true-triaxial compression. *J. Geophys. Eng.* **2018**, *15*, 2021–2032.
32. Kachanov, L. Time of the rupture process under creep conditions. *Izv. Akad. Nauk. SSR Otd. Tech. Nauk.* **1958**, *8*, 26–31.
33. Rabotnov, Y. On the equation of state for creep. *Prog. Appl. Mech.* **1963**, *178*, 307–315.
34. Wang, J.; Yang, A.; Liu, S.; Zheng, J. Improved fast algorithm to calculate correlation dimension of time series. *J. Huazhong Univ. Sci. Technol. (Nat. Sci. Ed.)* **2010**, *40*, 101–104.
35. Gai, Q.; Gao, Y.; Zhang, X.; He, M. A new method for evaluating floor spatial failure characteristics and water inrush risk based on microseismic monitoring. *Rock Mech. Rock Eng.* **2024**, *56*, 6481–6501. [[CrossRef](#)]
36. Cao, W.; Durucan, S.; Cai, W.; Shi, J.; Korre, A.; Jamnikar, S.; Rošer, J.; Lurka, A.; Siata, R. The role of mining intensity and pre-existing fracture attributes on spatial, temporal and magnitude characteristics of microseismicity in longwall coal mining. *Rock Mech. Rock Eng.* **2020**, *53*, 4139–4162. [[CrossRef](#)]

Disclaimer/Publisher’s Note: The statements, opinions and data contained in all publications are solely those of the individual author(s) and contributor(s) and not of MDPI and/or the editor(s). MDPI and/or the editor(s) disclaim responsibility for any injury to people or property resulting from any ideas, methods, instructions or products referred to in the content.